The CD45+ fraction in murine adipose tissue derived stromal cells harbors immune-inhibitory inflammatory cells

The CD45^{+} fraction in murine adipose tissue-derived stromal cells harbors immune-inhibitory inflammatory cells

Alessandro Nasti[1, *], Yoshio Sakai[2, 3, *], Akihiro Seki[1], Geraldine Belen Buffa[1], Takuya Komura[2], Hatsune Mochida[1], Masatoshi Yamato[1], Keiko Yoshida[1], Tuyen T. B. Ho[3], Masayuki Takamura[4], Soichiro Usui[2], Takashi Wada[2], Masao Honda[3], Shuichi Kaneko[1, 2, 3].

[1] Disease Control and Homeostasis, Graduate School of Medical Sciences, Kanazawa University.

[2] School of Medicine, College of Medical, Pharmaceutical, and Health Sciences, Kanazawa University.

[3] Department of Gastroenterology, Kanazawa University Hospital.

[4] Department of Cardiology, Kanazawa University Hospital.

Correspondence: Shuichi Kaneko, M.D., Ph.D., School of Medicine, College of Medical, Pharmaceutical, and Health Sciences, Kanazawa University, 13-1 Takara-machi, Kanazawa, Ishikawa 920-8641, Japan. Phone: +81-76-265-2233, FAX: +81-76-234-4250, e-mail: skaneko@m-kanazawa.jp

Keywords: Adipose tissue, stromal cells, immune inhibition, M2 macrophage, repair/regenerative therapy

Abbreviations: u-ADSCs: uncultured adipose-derived stromal cells, ConA: concanavalin A, MSCs: mesenchymal stem cells, c-ADSCs: cultured adipose tissue-derived stem cells, PBCs:

peripheral blood cells, SPCs: splenocytes, BMCs: bone marrow cells, qRT-PCR: real-time quantitative reverse-transcription polymerase chain reaction, LPS: lipopolysaccharides

*These authors contributed equally to this work.

Abstract

Stromal cells in adipose tissue are useful for repair/regenerative therapy as they harbor a substantial number of mesenchymal stem cells; therefore, freshly isolated autologous uncultured adipose tissue-derived stromal cells (u-ADSCs) are useful for regenerative therapy, and obviate the need for mesenchymal stem cells. We evaluated the therapeutic effect of murine u-ADSCs and the sorted subsets of u-ADSCs in a concanavalin A (ConA)-induced murine model of hepatitis, as well as their characteristics. We found that 10% to 20% of u-ADSCs expressed the CD45 leukocyte-related antigen. CD68, which is a marker of macrophages, was expressed by 50% of $CD45^+$ u-ADSCs. About 90% of $CD68^+CD45^+$ cells expressed CD206 antigen, which is a marker of inhibitory M2-type macrophages. Genes related to M2-type macrophages were more highly expressed by $CD45^+$, especially $CD45^+/CD206^+$, than by $CD45^-$ u-ADSCs. $CD45^+$ u-ADSCs inhibited the expression of cytokines/chemokines and suppressed the proliferation of splenocytes stimulated with ConA. We observed that not only whole u-ADSCs, but also the $CD45^+$ subset of u-ADSCs ameliorated the ConA-induced hepatitis in mice. In conclusion, freshly isolated murine u-ADSCs were effective against acute hepatitis, and $CD45^+$ u-ADSCs, phenotypically and functionally M2-type macrophage-like, contributed to the repair of liver tissue undergoing inflammation.

Introduction

Repair/regenerative therapy of impaired organs using stem cells has been a focus of research, while stem cells themselves have also been investigated intensively [1]–[3]. Various stem cell types have been discovered, for example, toti-potent stem cells, such as embryonic stem (ES) cells and induced pluripotent stem cells (iPS cells), and somatic stem cells, including tissue-resident stem cells and multi-potent mesenchymal stem cells (MSCs). MSCs are the ideal stem cells as they naturally reside in the adult body. In addition, they inhibit the immune system, which facilitates the repair and restoration of organs damaged by inflammation [4]–[6]. Bone marrow and adipose tissue are useful for repair/regenerative therapy as a feasible autologous source, since stromal cells in these tissues are naturally enriched in MSCs, avoiding advanced techniques for obtaining stem cells as of induced pluripotent stem cells [7],[8] and are not associated with serious ethical issues, such as the destruction of embryos for the establishment of ES cells. Subcutaneous adipose tissue is an attractive source of MSCs; adipose tissue contains approximately 100-fold more MSCs than bone marrow [9],[10]. In addition, subcutaneous adipose tissue is readily accessible to the aspiration of stromal cells enriched with MSCs [10]. Thus, freshly isolated stromal cells are useful for the repair/regenerative therapy of damaged tissue [11]–[13].

Non-clinical [14] and clinical studies using freshly isolated bone marrow and adipose tissue-derived stromal cells for the therapy of impaired organs have been reported [15]–[17]. Stromal cells from bone marrow and adipose tissues contain a substantial number of MSCs and a heterogeneous cellular composition—adipose tissue contains not only MSCs but also fibroblasts, endothelial cells, and leukocytes, among others [18],[19]. Analysis of subfractions of freshly isolated and uncultured adipose tissue-derived stromal cells (u-ADSCs) would enable determination of their biological characteristics.

In the current study, u-ADSCs and the subsets of them, $CD45^+$ u-ADSCs and $CD45^-$

u-ADSCs, ameliorated concanavalin A (ConA)-induced damage to murine liver tissue. By analyzing surface antigen expression, we found that among the $CD45^+$ subset of u-ADSCs, half of them were phenotypically similar to M2-type macrophages. This was confirmed by gene expression profile data and suppressive effect against proliferation of ConA-stimulated splenocytes *in vitro*. Thus, the immunosuppressant effect of treatment of inflamed tissues with freshly isolated u-ADSCs is attributable to some extent to the $CD45^+$ fraction.

Results

Characteristics of u-ADSCs

Stromal cells were isolated from the inguinal adipose tissue of C57BL/6J mice. The expression of surface antigens by u-ADSCs and cultured adipose tissue-derived stem cells (c-ADSCs) obtained by the expansion of u-ADSCs was determined. The u-ADSCs contained a higher frequency of cells expressing CD45 (10% to 20%) and CD31 (56.6%) than did c-ADSCs. In addition, u-ADSCs harbored cells expressing CD29 (35.5%), CD44 (47.3%), and CD90 (25.3%), confirming the presence of MSCs antigens; after culturing, the frequency of these antigens in c-ADSCs became highly expressed: CD29 (98.3%), CD44 (93.8%), and CD90 (77.1%) (Fig. 1A, B). The average sizes of the u-ADSCs and c-ADSCs were 11.3 ± 4.0 μm (SD) (n = 1868) and 27.6 ± 7.9 μm (SD) (n = 533), respectively (Fig. 1C).

Therapeutic effect of u-ADSC, $CD45^+$ u-ADSCs and $CD45^-$ u-ADSCs in ConA hepatitis mice

We previously reported that cultured and expanded c-ADSCs were effective in murine ConA hepatitis [20]. Thus, we determined the effect on ConA hepatitis of freshly isolated u-ADSCs, the source of c-ADSCs, as well as the u-ADSCs subsets which were enriched by using FACS (Supplemental fig. 1). The u-ADSCs, $CD45^+$ u-ADSCs, $CD45^-$ u-ADSCs, c-ADSCs and SPCs (control) were administered via the tail vein 3 h after ConA injection. Sixteen hours after ConA administration, liver tissues and sera were assessed. In terms of macroscopic appearance, livers were more intact in mice treated with u-ADSCs, $CD45^+$ u-ADSCs, $CD45^-$ u-ADSCs or c-ADSCs compared to the control group; consistently, upon microscopic observation, the liver tissues in the above mentioned groups showed no evidence of necrosis (data not shown). The u-ADSC, $CD45^+$ u-ADSCs and $CD45^-$ u-ADSCs treatments inhibited the ConA-induced infiltration of immune-mediating $CD11b^+$, $Gr\text{-}1^+$ and

F4/80$^+$ cells (Fig. 2A, B); no difference was detected with regard to the infiltration of CD4$^+$ or CD8$^+$ T cells in the livers between treatments. The serum ALT, and LDH activity levels were lower in the u-ADSCs, CD45$^+$ u-ADSCs, CD45$^-$ u-ADSCs and in c-ADSCs treatment groups than in SPCs (control group) (Fig. 2C). We also measured the cytokine concentration in the same sera. No significant difference of IFNg and TNF concentration was shown in any groups; however immunosuppressive cytokine, IL-10, tended to be slightly increased in the CD45$^+$ u-ADSC treatment group (Supplemental Fig. 2A). Instead, we observed significant decrease of *Ifng* and increase of *Il10* expression in the liver tissues of ConA hepatitis mice which were treated with CD45$^+$ u-ADSCs (Supplemental Fig. 2B).

CD45$^+$ u-ADSCs have a M2 macrophage-like phenotype

Freshly isolated u-ADSCs were effective against ConA hepatitis due to their immunosuppressive effect. We also found that the subset expressing CD45, leukocyte lineage antigen, were effective. To characterize the CD45$^+$ subset of u-ADSCs in details, we firstly compared the antigen-phenotypic features of the CD45$^+$ fraction with those of the CD45$^+$ fractions of peripheral blood cells (PBCs), splenocytes (SPCs), and bone marrow cells (BMCs) (Fig. 3A, B). Of the CD45$^+$ u-ADSCs, 50% expressed CD68 (Fig. 3B), suggestive of a macrophage phenotype [21], and almost 90% of them co-expressed CD206, suggestive of an M2 phenotype [22]–[24] (Fig. 3D). Furthermore, u-ADSCs, c-ADSCs, and the FACS sorted CD45$^+$ PBCs, CD45$^+$ SPCs, CD45$^+$ uADSCs, CD45$^-$ u-ADSCs, CD45$^+$/CD206$^+$ u-ADSCs, CD45$^+$/CD206$^-$ u-ADSCs, CD45$^+$/CD68$^+$ u-ADSCs, CD45$^+$/CD68$^-$ u-ADSCs fractions were assessed for the expression of genes related to M1- and M2-type macrophages by real-time quantitative reverse-transcription polymerase chain reaction (qRT-PCR). The expression of genes associated with M1-type macrophages—*Il1b*, *Tnf*, *Il23a*, *Cd80*, *Il6*, *Nos2*, *Il12a*, and *Il12b*—was downregulated in CD45$^+$ u-ADSCs compared with that in

$CD45^+$ PBCs and SPCs (Fig. 4A). In contrast, most M2-type genes (*Retnla*, *Arg1*, *Mrc1*, *Ccl22* and *Ccl24*) were upregulated in $CD45^+$ u-ADSCs (Fig. 4B). Among the subsets of $CD45^+$ u-ADSCs, only the $CD45^+/CD206^+$ u-ADSCs highly expressed the M2-type genes, not $CD45^+/CD206^-$ u-ADSCs, $CD45^+/CD68^+$ u-ADSCs, or $CD45^+/CD68^-$ u-ADSCs. The gene expression profile of c-ADSCs were not indicative of M2 macrophage.

Gene expression profile of $CD45^+$ and $CD45^-$ u-ADSCs

$CD45^+$ and $CD45^-$ u-ADSCs were subjected to gene expression analysis. A total of 8086 genes with a fold change > 4 (P-value <0.01, variance >2.6) were identified (Fig. 5A), of them, 2884 genes were upregulated and 3838 were downregulated in $CD45^+$ u-ADSCs compared with their expression levels in $CD45^-$ u-ADSCs. Pathway enrichment analysis (Fig. 5B) and biological process enrichment analysis (Fig. 5C) of these genes showed that $CD45^+$ u-ADSCs were related to activation and regulation of the immune response, regulation of leukocyte-mediated immunity, and cytokine/chemokine signaling pathways. In contrast, the $CD45^-$ fraction was related to developmental and morphogenic activation, cell matrix organization, ECM-receptor interactions, and structure organization (Fig. 5B, C). The expression of genes representative of M1- or M2-type macrophages was also evaluated; M1-macrophage-related genes were downregulated in $CD45^+$ u-ADSCs (Fig. 6A), and murine M2-macrophage specific genes were upregulated [23] (Fig. 6B).

$CD45^+$ u-ADSCs, and $CD45^+/CD206^+$ u-ADSCs suppressed activated SPCs *in vitro*

To assess the immune-modulatory function of $CD45^+$ u-ADSCs, freshly isolated splenocytes were co-cultured with $CD45^+$ u-ADSCs or total u-ADSCs in medium containing ConA. Two hours later, splenocytes in the culture insert were collected, and subjected to RNA isolation and gene expression analysis by qRT-PCR. The u-ADSCs significantly

suppressed the expression of *Ccl3* (Fig. 7A) and *Tnf* (Fig. 7C); in addition, $CD45^+$ u-ADSCs suppressed the expression of not only *Ccl3* (Fig. 7A) and *Tnf* (Fig. 7C), but also *Ifng* (Fig. 7B) by splenocytes. We also performed [^{3}H]-Thymidine incorporation assay; irradiated $CD45^+$ u-ADSCs or $CD45^+/CD206^+$ u-ADSCs were co-cultured with ConA-stimulated splenocytes for 24 hours, followed by 16 hours of pulsing with [^{3}H]-Thymidine; then the extent of [^{3}H]-Thymidine incorporation was measured by radioactivity counter. The $CD45^+$ subset of u-ADSCs and the $CD45^+/CD206^+$ fraction suppressed the proliferation of splenocytes stimulated with ConA (Fig. 7D).

IL-10-producing ability of u-ADSCs, $CD45^+$, and $CD45^+/CD206^+$ of u-ADSCs.

IL-10 is the important cytokine produced by M2 macrophage. Therefore, we assessed *Il10* expression of u-ADSC and their subsets under basal and activation conditions by gene expression analysis, as well as the frequency of cells which were intracellularly stained for IL-10 assessed by flow cytometry. Freshly isolated u-ADSCs, $CD45^+$ u-ADSCs, $CD45^-$ u-ADSCs were stimulated with IL-4/IL-13 or lipopolysaccharides (LPS), for 40 hours followed by assessment of *Il10* gene expression by qRT-PCR. The whole u-ADSCs and $CD45^+$ u-ADSCs greatly expressed *Il10* in both IL-4/IL-13, and LPS-stimulated conditions, respectively, as well as in basal condition (Supplemental Fig. 3A); the $CD45^-$ u-ADSCs did not express detectable level of *Il10* by qRT-PCR. Next, we performed intracellular staining assay of IL-10. The freshly isolated u-ADSCs were cultured with IL-4/IL-13, or LPS; then, FACS analysis of cells co-stained with FITC anti-CD45, PE anti-CD206 and Alexa Fluor® 647 anti-IL10 antibodies were performed (Supplemental Fig. 3B). Frequencies of IL-10 expressing cells of the u-ADSCs under the basal condition, IL-4/IL-13 or LPS stimulant were 7.5%, 7.4% and 8.4%, respectively. The frequency of IL-10 expressing cells in $CD45^+$ u-ADSCs (8.4%) was slightly higher compared to $CD45^-$ u-ADSCs (7.2%) under basal

condition; when cells were cultured with stimulants, either IL4/IL-13 or LPS, the frequency of IL-10 expressing cells in the $CD45^+$ subset resulted in 10.6% by IL4/IL-13 and 10.7% by LPS, respectively; in contrast, the frequency of IL-10 expressing cells in $CD45^-$ u-ADSCs did not increase (5.4%, and 6.6% by IL-4/IL-13 and LPS stimulation, respectively). The IL-10 expressing cells of the $CD45^+/CD206^+$ u-ADSCs subset were 20.1% in basal condition, 32.6% with IL-4/IL-13, and 24.4% with LPS; these high IL-10 expressing frequencies further confirmed the M2-like character of this $CD45^+/CD206^+$ u-ADSCs subset. On the contrary, the $CD45^+/CD206^-$ u-ADSCs IL-10 expressing cells were 5.9% (basal), 6.6% (IL-4/IL-13) and 9.0% (LPS).

Discussion

Stromal cells of adipose tissue and bone marrow have potential for repair/regenerative therapy as they harbor pluripotent and immunosuppressive MSCs. Repair/regenerative therapy using cells freshly isolated from these tissues is preferable, as they are accessible and complicated procedures are not required to obtain cells enriched with MSCs. In the current study, we observed that u-ADSCs were therapeutically beneficial to hepatitis as c-ADSCs were [20], and a part of its mechanism was contributed by the $CD45^+$ subset of u-ADSCs; although the $CD45^-$ subset of u-ADSCs were also proven to contribute to therapeutic effect of u-ADSCs. We found that 10–20% of u-ADSCs expressed the $CD45^+$ leukocyte-related antigen, and the majority were phenotypically similar to macrophages, particularly M2 macrophages, in terms of surface antigen expression and gene expression profile; they were functionally immunosuppressive *in vitro* and *in vivo*, suggesting that they contributed to the therapeutic effects of u-ADSCs.

Stromal cells freshly isolated from adipose tissue include not only MSCs but also inflammatory cells, fibroblasts, and endothelial cells, among others [18],[19]. Thus, investigations should determine the cell types present and the suitability of their biological characteristics for repair/regenerative therapy. The majority of $CD45^+$ u-ADSCs was phenotypically similar to macrophages, specifically M2-type macrophages, which express CD206. Indeed, their upregulated expression of *Retnla*, *Egr2*, *Arg1*, *Mrc1*, *Ccl17*, and *Ccl22* supports their similarity to immune-suppressive M2-type macrophages [22],[23],[25]. Functionally, these M2-macrophage-like cells suppressed splenocytes stimulated by ConA *in vitro*, expressed high level of IL-10, and showed immunosuppressive activity in a murine model of inflammation-related liver damage *in vivo*. Thus, inhibitory inflammatory cells, specifically those similar to M2-type macrophages, are present among $CD45^+$ u-ADSCs from enzymatically digested adipose tissue. A previous phenotypic analysis of human adipose

tissue-derived stromal cells showed that hematopoietic stem cells harbored M2-like anti-inflammatory cells, and were likely derived from myeloid tissue [26]. We functionally identified inhibitory inflammatory cells among leukocyte-related-antigen-expressing u-ADSCs. Moreover, macrophages obtained from murine bone marrow are useful for the treatment of inflammation and fibrosis, and for liver regeneration, in an animal model [27], as was the $CD45^+$ fraction in this study. Although macrophages have diverse biological characteristics [28], their fraction has been shown to be critically involved in repair, tissue development, and homeostasis [29].

We previously observed that ConA hepatitis was mediated by monocyte/macrophage lineage cells and $CD4^+$ T cells in part [20]. In the current study, we observed that infiltration of $CD11b^+$ cells in the liver of ConA hepatitis were decreased, but not $CD4^+$ T cells. However, T cell-related cytokines such as IL-10 and IFNg expression in the liver of ConA hepatitis mice treated with $CD45^+$ u-ADSCs were increased and decreased, respectively, implying that it is possible that $CD4^+$ T cells were functionally affected by $CD45^+$ u-ADSCs treatment. The details on how u-ADSCs and their subsets are immune-suppressive to ConA hepatitis should be further investigated. About half of $CD45^+$ u-ADSCs were not phenotypically macrophage in the context of surface antigen expression as well as gene expression profile. The biological characteristics of these "non-macrophage" $CD45^+$ u-ADSCs should be further investigated on how they contribute to immune-suppression to ConA hepatitis mice *in vivo*. Furthermore, the subset $CD45^-$ of u-ADSCs were also therapeutically effective to acute hepatitis, and they should be explored, especially in the context of the fraction containing mesenchymal stem cells which are immune-suppressive to inflammation.

In conclusion, the entire u-ADSC population can be used to treat damaged tissue [18],[30]–[36]; they contain a substantial number of MSCs and they enable the repair and

restoration of inflammation-mediated liver damage. These cells include an immune-suppressive macrophage-phenotype subfraction, which contributes to amelioration of inflammation-mediated tissue damage. Freshly isolated u-ADSCs are advantageous compared to c-ADSCs, since they do not require manufacturing process or culture; these factors presumably facilitate the application to clinical use [37],[38]. Thus, adipose-tissue-derived stromal cells may be useful for the repair/restoration of damaged tissue.

Materials and Methods

Stromal cell isolation from murine inguinal subcutaneous adipose tissue

The inguinal adipose tissues of C57BL/6J male mice (12 to 16 weeks old) (Charles River Laboratories Japan, Yokohama, Japan) were digested using type I collagenase (Worthington Biochemical Corporation, Lakewood, NJ, USA). The stromal fraction was separated from adipocytes and fat-derived debris by centrifugation (350 g for 15 min); the supernatant was then discarded. As described previously [20], c-ADSCs were obtained by culturing u-ADSCs in medium comprising a 1:1 ratio of DMEM/F12 (Gibco, Life Technologies, Carlsbad, CA, USA) supplemented with 20% v/v heat-inactivated fetal bovine serum (Life Technologies) and 1% antibiotic–antimycotic solution (Life Technologies); the c-ADSCs were passaged five times and used for experiments. Our institutional review board approved the procedures for the care and use of laboratory animals in this study.

Isolation of splenocytes, peripheral blood cells, and bone marrow cells

Murine SPCs were isolated from C57BL/6J male mice as described previously [39]. To isolate PBCs, blood was withdrawn from anesthetized male C57BL/6J mice by cardiac puncture, placed in a heparin sodium vacutainer (Venoject II, VP-H100K; Terumo, Tokyo, Japan), diluted with an identical volume of PBS (Wako Pure Chemical Industries, Osaka, Japan), filtered through a 40 μm cell strainer (Corning Life Sciences, Durham, NC, USA), and centrifuged. Red blood cells were then lysed in ACK Lysing Buffer (Lonza, Walkersville, MD, USA) and the supernatant was discarded. Bone marrow cells (BMCs) were extracted from the femoral bone of male C57BL/6J mice.

Flow cytometry

Freshly extracted u-ADSCs or c-ADSCs were incubated in PBS supplemented with 2% v/v FBS (Gibco, Life Technologies) for 10 min at 4°C with murine FcR Blocking Reagent (Miltenyi Biotec GmbH, Bergisch Gladbach, Germany). Cells were then washed, incubated with fluorescence-labeled antibodies, and analyzed using a FACSCalibur® cytometer (BD Biosciences, Franklin Lakes, NJ, USA). The following antibodies were used: FITC-labeled rat anti-mouse CD45 (clone 30-F11) (BD Pharmingen, San Jose, CA, USA), PE-anti-mouse CD34 (clone HM34), PerCP/Cy5.5-anti-mouse CD68 (clone FA-11), APC-anti-mouse CD206 (MMR) (clone C068C2) (Biolegend, San Diego, CA, USA), FITC-hamster anti-rat CD29 (clone Ha2/5) (BD Pharmingen), PE-anti-mouse CD73 (clone TY/11.8) (Biolegend), FITC-anti-human/mouse CD44 (clone IM7) (eBioscience, San Diego, CA, USA), PE-anti-mouse CD105 (clone MJ7/18) (Miltenyi Biotec, Tokyo, Japan), PE-anti-mouse CD31 (clone 390) (Beckman Coulter, Brea, CA, USA), and PE-anti-mouse CD90 (clone G7) (Novus Biologicals, Littleton, CO, USA). Data were analyzed using FlowJo® V10 software (Tree Star, Ashland, OR, USA).

Cell size characterization

Micrographs of u-ADSCs and c-ADSCs in suspension were obtained and analyzed using ImageJ software (NIH, Bethesda, MD, USA) [40].

Cell sorting

Freshly isolated u-ADSCs, PBCs, or SPCs were filtered through a 100 μm mesh (Corning Life Sciences, Durham, NC, USA) and then through a 40 μm cell strainer, and suspended in sorting buffer: PBS supplemented with 2% w/v bovine serum albumin (Sigma-Aldrich, St. Louis, MO, USA), 25 mM HEPES (Dojindo Molecular Technologies, Inc., Kumamoto, Japan), and 5 mM EDTA (Nippon Gene Co., Tokyo, Japan). Cells were

centrifuged and the supernatant aspirated. The obtained cells were incubated with murine FcR Blocking Reagent (Miltenyi Biotec) for 10 min at 4°C, washed, and incubated for a further 10 min at 4°C with FITC-labeled rat anti-mouse CD45 and 7-amino-actinomycin D (BD Biosciences). The labeled cells were sorted using a FACS ARIA II® cytometer (BD Biosciences) (Supplemental Fig. 1).

Treatment of acute ConA-induced hepatitis with u-ADSCs, $CD45^+$ u-ADSCs or $CD45^-$ u-ADSCs

C57Bl/6J male mice (24 weeks old) were injected with ConA (20 mg/kg) (Wako) in PBS (200 µl) via the tail vein, as described previously [20]. Three hours later, 7.5×10^5 cells were injected in a volume of 100 µl of PBS into the tail vein for each treatment groups: u-ADSCs, $CD45^+$ u-ADSCs, $CD45^-$ u-ADSCs and SPCs (control). For the c-ADSCs treatment group, the injected cells were fixed to 1×10^5 cells in order to avoid thromboembolism. Sixteen hours later, the mice were euthanized, and blood sera and liver tissues were sampled.

Histological and immunohistochemical analyses

Liver tissue was fixed in IHC Zinc Fixative® (BD Pharmingen) for paraffin embedding. Tissue sectioning, deparaffinization, epitope retrieval, and peroxidase and protein blockings were performed as described previously [20]. Rat anti-mouse CD4 (clone H129.19), CD8a (clone 53-6.7), CD11b (clone M1/70), Gr-1 (clone RB6-8C5) (BD Pharmingen), F4/80 (clone BM8) (Invitrogen, Life Technologies, Camarillo, CA, USA) and primary antibodies were used. Tissues were incubated with the primary antibodies in PBS containing 1% BSA and stored overnight at 4°C. After washing in PBS, the anti-rat detection reagent Histofine Simple Stain Mouse MAX PO® (Nichirei Corporation, Tokyo, Japan) was applied, followed by incubation for 30 min at room temperature. Hydrogen peroxide solution

containing imidazole-HCl buffer was then applied, followed by 3,3′-diaminobenzidine substrate solution (Dako ChemMate EnVision Kit / HRP (DAB)®) (Dako, Kyoto, Japan) to visualize immune complexes; finally, hematoxylin was applied as a counterstain.

Co-culture of ConA-stimulated splenocytes with u-ADSCs

SPCs isolated from C57BL/6J male mice were suspended in medium composed of RPMI 1640 (Gibco, Life Technologies), 10% v/v heat-inactivated FBS, and 10 μg/ml ConA, and plated in 24-well plates at 2.44×10^6 cells/ml in triplicate (3×10^5 cells/well) (BD Falcon). Suspensions of u-ADSCs or $CD45^+$ u-ADSCs (5×10^5 cells/well) were placed in culture insert wells (BD Falcon Cell Culture Inserts) and co-cultured with SPCs. Two hours later, the inserts harboring u-ADSCs or fractioned cells were removed, and SPCs were lysed for RNA extraction.

[^{3}H]-Thymidine incorporation assay

SPCs (5×10^5 cells) were co-seeded in a 96 well plate-round bottom with either 3×10^5 irradiated (5000 rad) u-ADSCs or irradiated (5000 rad) u-ADSCs subsets in triplicates. RPMI complete medium (150 μl) was used with or without ConA as stimulant (5 μg/mL); then, incubated for 24 h at 37°C, followed by pulsing with 1 μCi/well of [^{3}H]-Thymidine for 16 h. Cells were harvested by centrifugation and were washed twice with PBS. The harvested cells were suspended in Clear-sol I® liquid scintillation (Nacalai Tesque, Kyoto, Japan) and radioactivity was quantified with the LSC-5100® liquid scintillation counter (Aloka, Tokyo, Japan).

Activation of u-ADSCs by stimulants for macrophage subsets and intracellular staining

Freshly isolated u-ADSCs, $CD45^+$ u-ADSCs and $CD45^-$ u-ADSCs (3×10^5 cells) were seeded in triplicates and cultured for 40 hours with, (i) 20 ng/mL of recombinant murine IL-4 (PeproTech, NJ, USA) plus 20 ng/mL of recombinant murine IL-13 (R&D Systems, MN, USA), (ii) 50 ng/mL of LPS (Sigma-Aldrich), or (iii) kept in RPMI1640 culture media without any stimulants as basal condition; cells were lysed for RNA isolation, and the expression of *Il10* was assessed by qRT-PCR. For assessing the frequency of the IL-10 expressing cells for each subset, 1×10^6 freshly isolated u-ADSCs were seeded in triplicates and cultured, as above mentioned, for 40 hours with IL-4/IL-13, LPS or, kept in basal condition. Cells were harvested, co-stained with FITC anti-CD45 and PE anti-CD206, followed by fixation, permeabilization, and incubated with Alexa Fluor® 647 anti-IL10 (clone JES5-16E3) (Biolegend) using Inside Stain Kit® (Miltenyi Biotec); FACS data was collected with the BD Accuri™ C6 Cytometer (BD Biosciences), the frequency of IL-10-stained cells was quantified by FACS analysis.

Serologic analysis and serum cytokine concentrations measurement

Blood was collected from mice from the venous plexus in the retro-orbital space, serum was separated from clotted blood by centrifugation, ALT and LDH activities were measured as described previously [20]. The same sera was also used for assessing the concentrations of cytokines by using the Bio-Plex Pro™ cytokine assay kit (Bio-Rad Laboratories, Hercules, CA, USA) following the manufacturer's protocol.

Real-time quantitative reverse-transcription polymerase chain reaction (qRT-PCR)

A High Pure RNA Isolation Kit® (Roche Diagnostics GmbH, Mannheim, Germany) was used for total RNA purification as per the manufacturer's protocol. Single-stranded cDNA was synthesized from RNA using reverse transcriptase (Applied Biosystems,

Waltham, MA, USA) following the supplier's protocol. Real-time qPCR was performed with the Applied Biosystems® 7900HT Fast Real-Time PCR System instrument following the manufacturer's protocol. cDNA was mixed with qPCR MasterMix Plus® (Eurogentec, Seraing, Belgium) and the following hydrolysis TaqMan® Gene Expression Assay probes (Applied Biosystems): Tnf, Ifng, Ccl3, Il1b, Ccl2, Cxcl10, Il6, Nos2, Il12a, Il12b, Il23a, Cd80, Mrc1, Cd163, Retnla, Arg1, Il10, Ccl22, and Ccl24.

DNA microarray analysis

RNAs were isolated, amplified, and labeled with Cy3 using a Quick Amp Labeling Kit following the manufacturer's protocol (Agilent Technologies, Santa Clara, CA, USA). Complementary RNA was hybridized on a Whole Mouse Genome 4 × 44K Array (Agilent Technologies). A DNA microarray scanner (model G2505B, Agilent Technologies) was used to read microarrays. Gene expression analysis was performed using the BRB array tool (http://linus.nci.nih.gov/BRB-ArrayTools.html), quantile normalization was applied. Data are from one test per cell population; gene pool subsets were selected based on the canonical M1 and M2 macrophage gene signatures, and newly identified murine genes in the Gene Expression Omnibus NCBI database (GSE69607) [23]. Comprehensive functional analysis of gene lists was performed using DAVID Bioinformatics Resources 6.7 (https://david.ncifcrf.gov/) [41].

Statistical analysis

Data are expressed as means ± SD, unless stated otherwise. OriginPro 8 SR0 (v8.0724; OriginLab Corporation, Northampton, MA, USA) was used for graphing and data analysis. GraphPad was used for unpaired two-tailed t-test (http://graphpad.com/quickcalcs/, GraphPad Software, La Jolla, CA, USA), R package was used for the Kruskal-Wallis test and

R package Pairwise Multiple Comparison of Mean Ranks Package (PMCMR) for the *post-hoc* tests [42].

Acknowledgements: We sincerely thank Ms. Sachie Yamazaki, Ms. Mahoko Yoshita, Ms. Ayana Takeuchi and Ms. Mei Awaji for technical assistance. This work was supported in part by a grant from the Japan Society for the Promotion of Science.

Conflict of interest: The authors declare no commercial or financial conflict of interest.

References

1. **Leeper, N. J., Hunter, A. L., Cooke, J. P.,** Stem cell therapy for vascular regeneration: Adult, embryonic, and induced pluripotent stem cells. *Circulation*. 2010. **122**: 517–526.

2. **Schuleri, K. H., Boyle, A. J., Hare, J. M.,** Mesenchymal stem cells for cardiac regenerative therapy. **In Kauser, K., Zeiher, A-M., (Eds.)** Bone marrow-derived progenitors. Berlin, Heidelberg: Springer Berlin Heidelberg; 2007, pp 195–218.

3. **Enzmann, V., Yolcu, E., Kaplan, H., Ildstad, S.,** Stem cells as tools in regenerative therapy for retinal degeneration. *Arch. Ophthalmol.* 2009. **127**: 563–571.

4. **Pittenger, M. F., Mackay, A. M., Beck, S., Jaiswal, R. K., Douglas, R., Mosca, J. D., Moorman, M. A. et al.,** Multilineage potential of adult human mesenchymal stem cells. *Science*. 1999. **284**: 143–147.

5. **Ren, G., Zhang, L., Zhao, X., Xu, G., Zhang, Y., Roberts, A. I., Zhao, R. C. et al.,** Mesenchymal stem cell-mediated immunosuppression occurs via concerted action of chemokines and nitric oxide. *Cell Stem Cell*. 2008. **2**: 141–150.

6. **Yang, M., Li, Q., Sheng, L., Li, H., Weng, R., Zan, T.,** Bone marrow–derived mesenchymal stem cells transplantation accelerates tissue expansion by promoting skin regeneration during expansion. *Ann. Surg.* 2011. **253**: 202–209.

7. **Hanna, J., Wernig, M., Markoulaki, S., Sun, C-W., Meissner, A., Cassady, J. P., Beard, C. et al.,** Treatment of sickle cell anemia. *Science*. 2007. **1920**: 1920–1923.

8. **Park, I. H., Lerou, P. H., Zhao, R., Huo, H., Daley, G. Q.,** Generation of human-induced pluripotent stem cells. *Nat Protoc*. 2008; **3**: 1180–1186.

9. **Aust, L., Devlin, B., Foster, S. J., Halvorsen, Y. D. C., Hicok, K., du Laney, T., Sen, A. et al.,** Yield of human adipose-derived adult stem cells from liposuction aspirates. *Cytotherapy*. 2004. **6**: 7–14.

10. **Zuk, P. A., Zhu, M., Mizuno, H., Huang, J., Futrell, J. W., Katz, A. J., Benhaim, P.**

et al., Multilineage cells from human adipose tissue: implications for cell-based therapies. *Tissue Eng.* 2001. **7**: 211–228.

11. **Varma, M. J. O., Breuls, R. G. M., Schouten, T. E., Jurgens, W. J. F. M., Bontkes, H. J., Schuurhuis, G. J., Ham, S. M. V. et al.,** Phenotypical and functional characterization of freshly isolated adipose tissue-derived stem cells. *Stem Cells Dev.* 2007. **16**: 91–104.

12. **Dahl, J-A., Duggal, S., Coulston, N., Millar, D., Melki, J., Shahdadfar, A., Brinchmann, J. E. et al.,** Genetic and epigenetic instability of human bone marrow mesenchymal stem cells expanded in autologous serum or fetal bovine serum. *Int. J. Dev. Biol.* 2008. **52**: 1033–42.

13. **Jones, E., English, A., Churchman, S. M., Kouroupis, D., Boxall, S. A., Kinsey, S., Giannoudis, P. G. et al.,** Large-scale extraction and characterization of CD271+ multipotential stromal cells from trabecular bone in health and osteoarthritis: Implications for bone regeneration strategies based on uncultured or minimally cultured multipotential stromal cells. *Arthritis Rheum.* 2010. **62**: 1944–1954.

14. **Suganuma, S., Tada, K., Hayashi, K., Takeuchi, A., Sugimoto, N., Ikeda, K., Tsuchiya, H.,** Uncultured adipose-derived regenerative cells promote peripheral nerve regeneration. *J. Orthop. Sci.* 2013. **18**: 145–151.

15. **Henry, T. D., Pepine, C., Lambert, C., Traverse, J.H., Schatz, R., Costa, M., Povsic, T. J. et al.,** The Athena Trials: Autologous adipose-derived regenerative cells (ADRCs) for refractory chronic myocardial ischemia with left ventricular dysfunction. *Catheter. Cardiovasc. Interv.* 2017. **89(2)**: 169-177.

16. **Mizushima, T., Takahashi, H., Takeyama, H., Naito, A., Haraguchi, N., Uemura, M., Nishimura, J. et al.,** A clinical trial of autologous adipose-derived regenerative cell transplantation for a postoperative enterocutaneous fistula. *Surg. Today*. 2015. **46**: 835–842.

17. **Pérez-Cano, R., Vranckx, J. J., Lasso, J. M., Calabrese, C., Merck, B., Milstein, A.**

M., Sassoon, E. et al., Prospective trial of adipose-derived regenerative cell (ADRC)-enriched fat grafting for partial mastectomy defects: The RESTORE-2 trial. *Eur. J. Surg. Oncol.* 2012. **38**: 382–389.

18. **Yoshimura, K., Shigeura, T., Matsumoto, D., Sato, T., Takaki, Y., Aiba-Kojima, E., Sato, K. et al.,** Characterization of freshly isolated and cultured cells derived from the fatty and fluid portions of liposuction aspirates. *J. Cell. Physiol.* 2006. **208**: 64–76.

19. **Prunet-Marcassus, B., Cousin, B., Caton, D., André, M., Pénicaud, L., Casteilla, L.,** From heterogeneity to plasticity in adipose tissues: Site-specific differences. *Exp. Cell Res.* 2006. **312**: 727–736.

20. **Higashimoto, M., Sakai, Y., Takamura, M., Usui, S., Nasti, A., Yoshida, K., Seki, A. et al.,** Adipose tissue derived stromal stem cell therapy in murine ConA-derived hepatitis is dependent on myeloid-lineage and CD4+ T-cell suppression. *Eur. J. Immunol.* 2013. **43**: 2956–2968.

21. **Weisberg, S. P., McCann, D., Desai, M., Rosenbaum, M., Leibel, R. L., Ferrante Jr, A. W.,** Obesity is associated with macrophage accumulation in adipose tissue. *J. Clin. Invest.* 2003. **112**: 1796–1808.

22. **Martinez, F. O., Helming, L., Milde, R., Varin, A., Melgert, B. N., Draijer, C., Thomas, B. et al.,** Genetic programs expressed in resting and IL-4 alternatively activated mouse and human macrophages: Similarities and differences. *Blood*. 2013. **121**: 57–70.

23. **Jablonski, K. A., Amici, S. A., Webb, L. M., Ruiz-Rosado, J. D. D., Popovich, P. G., Partida-Sanchez, S., Guerau-De-arellano, M.,** Novel markers to delineate murine M1 and M2 macrophages. *PLoS One*. 2015. **10**: 5–11.

24. **Rabinowitz, S. S., Gordon, S.,** Macrosialin, a macrophage-restricted membrane sialoprotein differentially glycosylated in response to inflammatory stimuli. *J. Exp. Med.* 1991. **174**: 827–36.

25. **Mantovani, A.,** Macrophage diversity and polarization: in vivo veritas. *Blood*. 2006. **108**: 408–409.

26. **Eto, H., Ishimine, H., Kinoshita, K., Watanabe-Susaki, K., Kato, H., Doi, K., Kuno, S. et al.,** Characterization of human adipose tissue-resident hematopoietic cell populations reveals a novel macrophage subpopulation with CD34 expression and mesenchymal multipotency. *Stem Cells Dev*. 2013. **22**: 985–997.

27. **Thomas, J. A., Pope, C., Wojtacha, D., Robson, A. J., Gordon-Walker, T. T., Hartland, S., Ramachandran, P. et al.,** Macrophage therapy for murine liver fibrosis recruits host effector cells improving fibrosis, regeneration, and function. *Hepatology*. 2011. **53**: 2003–2015.

28. **Pollard, J. W.,** Trophic macrophages in development and disease. *Nat. Rev. Immunol.* 2009. **9**: 259–70.

29. **Davies, L. C., Jenkins, S. J., Allen, J. E., Taylor, P. R.,** Tissue-resident macrophages. *Nat Immunol*. 2013. **14**: 986–995.

30. **Mohammadi, R., Sanaei, N., Ahsan, S., Rostami, H., Abbasipour-Dalivand, S., Amini, K.,** Repair of nerve defect with chitosan graft supplemented by uncultured characterized stromal vascular fraction in streptozotocin induced diabetic rats. *Int. J. Surg.* 2014. **12**: 33–40.

31. **Semon, J. A., Zhang, X., Pandey, A. C., Alandete, S. M., Maness, C., Zhang, S., Scruggs, B. A. et al.,** Administration of murine stromal vascular fraction ameliorates chronic experimental autoimmune encephalomyelitis. *Stem Cells Transl. Med.* 2013. **2**: 789–796.

32. **Atalay, S., Coruh, A., Deniz, K.,** Stromal vascular fraction improves deep partial thickness burn wound healing. *Burns*. 2014. **40**: 1375–1383.

33. **Premaratne, G. U., Ma, L-P., Fujita, M., Lin, X., Bollano, E., Fu, M.,** Stromal vascular fraction transplantation as an alternative therapy for ischemic heart failure: Anti-

inflammatory role. *J. Cardiothorac. Surg.* 2011. **6**: 1–10.

34. **Han, S-K., Kim, H-R., Kim, W-K.,** The treatment of diabetic foot ulcers with uncultured, processed lipoaspirate cells: A pilot study. *Wound Repair Regen.* 2010. **18**: 342–348.

35. **Rigotti, G., Marchi, A., Galiè, M., Baroni, G., Benati, D., Krampera, M., Pasini, A. et al.,** Clinical treatment of radiotherapy tissue damage by lipoaspirate transplant: A healing process mediated by adipose-derived adult stem cells. *Plast. Reconstr. Surg.* 2007. **119**: 1409–1422.

36. **Jurgens, W. J. F. M., Kroeze, R. J., Zandieh-Doulabi, B., van Dijk, A., Renders, G. A. P., Smit, T. H., van Milligen, F. J. et al.,** One-step surgical procedure for the treatment of osteochondral defects with adipose-derived stem cells in a caprine knee defect: A pilot study. *Biores. Open Access*. 2013. **2**: 315–325.

37. **Sakai, Y., Takamura, M., Seki, A., Sunagozaka, H., Terashima, T., Komura, T., Yamato, M. et al.,** Phase I clinical study of liver regenerative therapy for cirrhosis by intrahepatic arterial infusion of freshly isolated autologous adipose tissue-derived stromal/stem (regenerative) cell. *Regen. Ther.* 2017. **6**: 52–64.

38. **Fraser, J. K., Hicok, K. C., Shanahan, R., Zhu, M., Miller, S., Arm, D. M.,** The Celution(R) System: Automated Processing of Adipose-Derived Regenerative Cells in a Functionally Closed System. *Adv. wound care*. 2014. **3**: 38–45.

39. **Kruisbeek, A. M.,** Isolation of mouse mononuclear cells. **In** Current protocols in immunology. John Wiley & Sons, Inc.; 2001. 3–1.

40. **Schneider, C. A., Rasband, W. S., Eliceiri, K. W.,** NIH Image to ImageJ: 25 years of image analysis. *Nat. Methods*. 2012. **9**: 671–675.

41. **Huang, D. W., Sherman, B. T., Lempicki, R. A.,** Bioinformatics enrichment tools: Paths toward the comprehensive functional analysis of large gene lists. *Nucleic Acids Res.*

2009. **37**: 1–13.

42. **Pohlert, T.,** The pairwise multiple comparison of mean ranks package (PMCMR). R package. 2014, pp 2004-2006.

Figure legends

FIGURE 1. Characteristics of u-ADSCs and c-ADSCs.

Freshly isolated u-ADSCs were obtained by digestion of the inguinal adipose tissue of C57BL/6J male mice, and were cultured to expand c-ADSCs. (A) Scattergrams of flow cytometry analysis of cells using fluorescence-conjugated antibodies to surface antigens. The data are representative of three independent experiments. (B) Frequency of u-ADSCs and c-ADSCs expressing surface markers. The data are representative of three independent experiments. Bars: SD. (C) The size distribution of u-ADSCs and c-ADSCs at passage 5 was assessed using ImageJ; relative FSC/SSC scatterplots are shown. The average sizes of u-ADSCs and c-ADSCs were 11.2 ± 4.0 μm (SD) (n = 1868) and 27.6 ± 7.9 μm (SD) (n = 533).

FIGURE 2. Therapeutic effect of u-ADSC administration in ConA hepatitis mice.

C57Bl/6J male mice were injected with ConA (20 mg/kg). Three hours later, the u-ADSCs, $CD45^+$ u-ADSCs, $CD45^-$ u-ADSCs, c-ADSCs or SPCs (control), were injected into the tail vein. Sixteen hours after the ConA injection, the mice were euthanized, and liver tissues and blood sera samples were obtained. (A) Immunohistochemical analysis of inflammatory cell markers (CD4, CD8, CD11b, Gr-1, F4/80) in liver tissue. One representative stain image of each group is presented. Magnification: ×100. Scale bars: 100 μm. The brown-stain of the inflammatory cells in the tissue sections (A) was quantified by using the colour deconvolution option of ImageJ (B); black bar: u-ADSCs treatment group; oblique line bar: $CD45^+$ u-ADSCs treatment group; diagonally hatched bar: $CD45^-$ u-ADSCs treatment group; dark gray/horizontal line bar: c-ADSCs treatment group; white/hatched bar: SPCs treatment group; (representative area analyzed = 1.576 mm^2). (C) At 16 h after ConA administration, serum ALT, and LDH activities were lower in the u-ADSC, $CD45^+$ u-ADSC, $CD45^-$ u-

ADSC and c-ADSC treatment groups than in the control group. Kruskal Wallis rank sum test followed by the Conover *post hoc* test was performed as statistical analysis. *P<0.05, **P<0.01; Treatment replicates: u-ADSC (n=6), $CD45^+$ u-ADSC (n=6), $CD45^-$ u-ADSC (n=4), c-ADSC (n=5) and SPCs (n=6).

FIGURE 3. Characteristics of the $CD45^+$ u-ADSCs.

The u-ADSCs, PBCs, SPCs, and BMCs were stained with the indicated antibodies and subjected to FACS analysis. (A) Frequency of $CD45^+$ u-ADSCs, compared with those of PBCs, SPCs, and BMCs. (B) Frequency of cells expressing surface markers of macrophages and MSCs among $CD45^+$ u-ADSCs, PBCs, SPCs, and BMCs. (A, B) Bars: SD. (C, D) Phenotypic characteristics of $CD45^+$ u-ADSCs. (C) Scattergram of FSCs and SSCs among the u-ADSCs. (D) Frequency of u-ADSCs expressing CD45 and CD68, and that of CD206-expressing $CD45^+CD68^+$ u-ADSCs. (A–D) All results are representative of two independent experiments.

FIGURE 4. Expression of M2-type macrophage-related genes in u-ADSCs and subsets.

The expression of genes representative of M1- or M2-type macrophages was assessed by qRT-PCR in freshly isolated cell populations. (A) Expression of M1-macrophage-related genes. (B) Expression of M2-macrophage-related genes. Figure abbreviations: PBC: $CD45^+$ PBCs; SPC: $CD45^+$ SPCs; $CD45^{pos}$: $CD45^+$ uADSCs; $CD45^{neg}$: $CD45^-$ u-ADSCs; $CD206^{pos}$: $CD45^+/CD206^+$ u-ADSCs; $CD206^{neg}$: $CD45^+/CD206^-$ u-ADSCs; $CD68^{pos}$: $CD45^+/CD68^+$ u-ADSCs; $CD68^{neg}$: $CD45^+/CD68^-$ u-ADSCs. Y-axis represents the relative gene expression normalized to *Gapdh*; bars: SD. All results are from three independent tests.

FIGURE 5. Biological process and pathway enrichment analysis of genes expressed by $CD45^+$ and $CD45^-$ u-ADSCs.

Gene expression analysis of $CD45^+$ and $CD45^-$ u-ADSCs was performed using DNA microarrays. (A) Scatterplot of fourfold upregulated and downregulated genes ($P < 0.01$, variance > 2.6) in $CD45^+$ u-ADSCs compared with $CD45^-$ u-ADSCs. Light gray line, fourfold change. The biological characteristics of the upregulated and downregulated genes were annotated and processed using DAVID Bioinformatics Resources 6.7. Pathway enrichment analysis (B) and biological process enrichment analysis (C) were conducted for genes upregulated in $CD45^+$ u-ADSCs compared with $CD45^-$ u-ADSCs (right-facing bars), and vice versa (left-facing bars). Bars represent −log(P-values); P-values were calculated by hypergeometric test (B, C).

FIGURE 6. Heatmap analysis of the expression of M1- and M2-type macrophage-related genes in $CD45^+$ u-ADSCs compared with that in control cells ($CD45^-$ u-ADSCs, PBCs, and SPCs) by DNA microarray. (A) M1-macrophage-related genes. (B) M2-macrophage-related genes. The data are from one test per cell population.

FIGURE 7. Immunosuppressive effects of $CD45^+$ u-ADSCs on activated splenocytes *in vitro*.

Freshly isolated splenocytes were co-cultured with total u-ADSCs or only $CD45^+$ u-ADSCs on culture inserts in medium containing ConA. Two hours later, the splenocytes were collected and subjected to RNA isolation and gene expression analysis by qRT-PCR. (A) *Ccl3*, (B) *Ifng*, (C) *Tnf*. A two-tailed t-test was used for statistical analysis. The data are representative of three independent experiments. (D) 5×10^5 SPCs were co-seeded with 3×10^5 irradiated u-ADSCs, $CD45^+$ u-ADSCs, or $CD45^+/CD206^+$ u-ADSCs in triplicates under

ConA stimulation; cells were co-cultured for 24 hours followed by 16 hours of pulsing with [^{3}H]-Thymidine; cells were harvested and radioactivity quantified. H-DPM: [^{3}H]-disintegrations per minute; n=3. Student t-test was performed. (A-D) *P<0.05, **P<0.01, ***P<0.001. Bars: SD.

Figures

FIGURE 1.

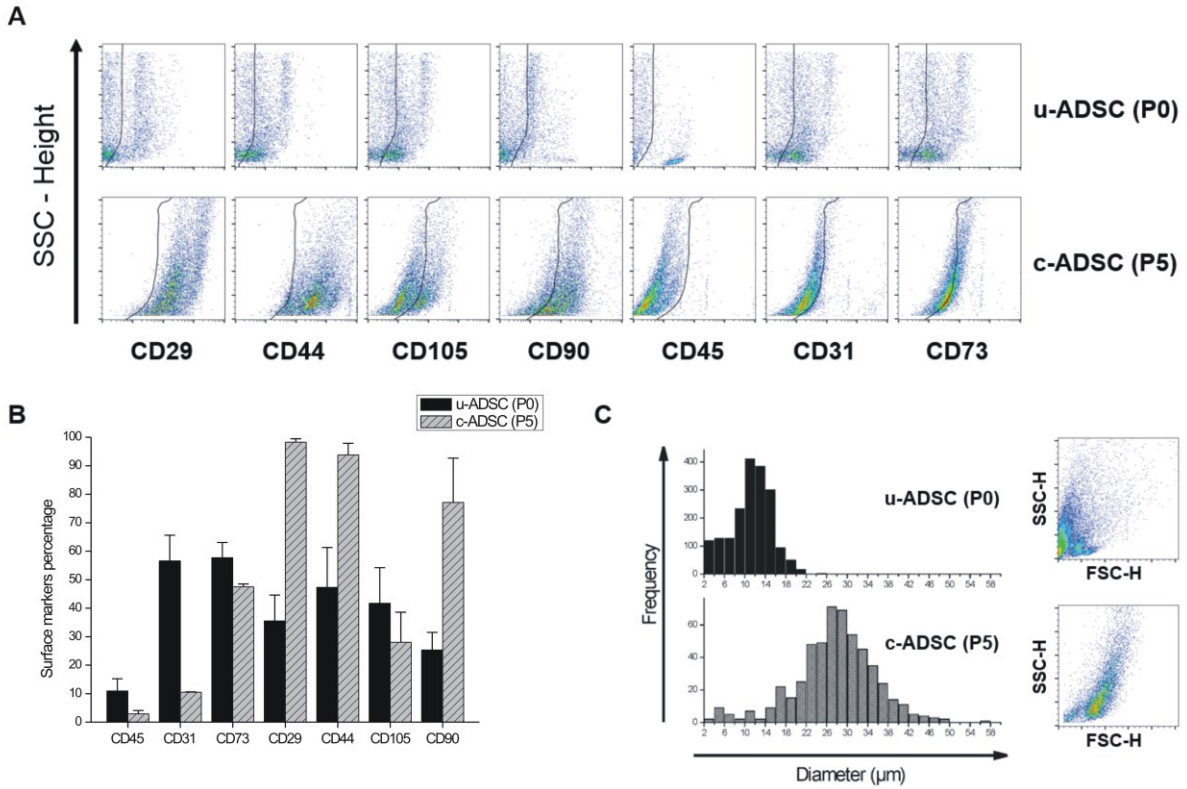

FIGURE 2.

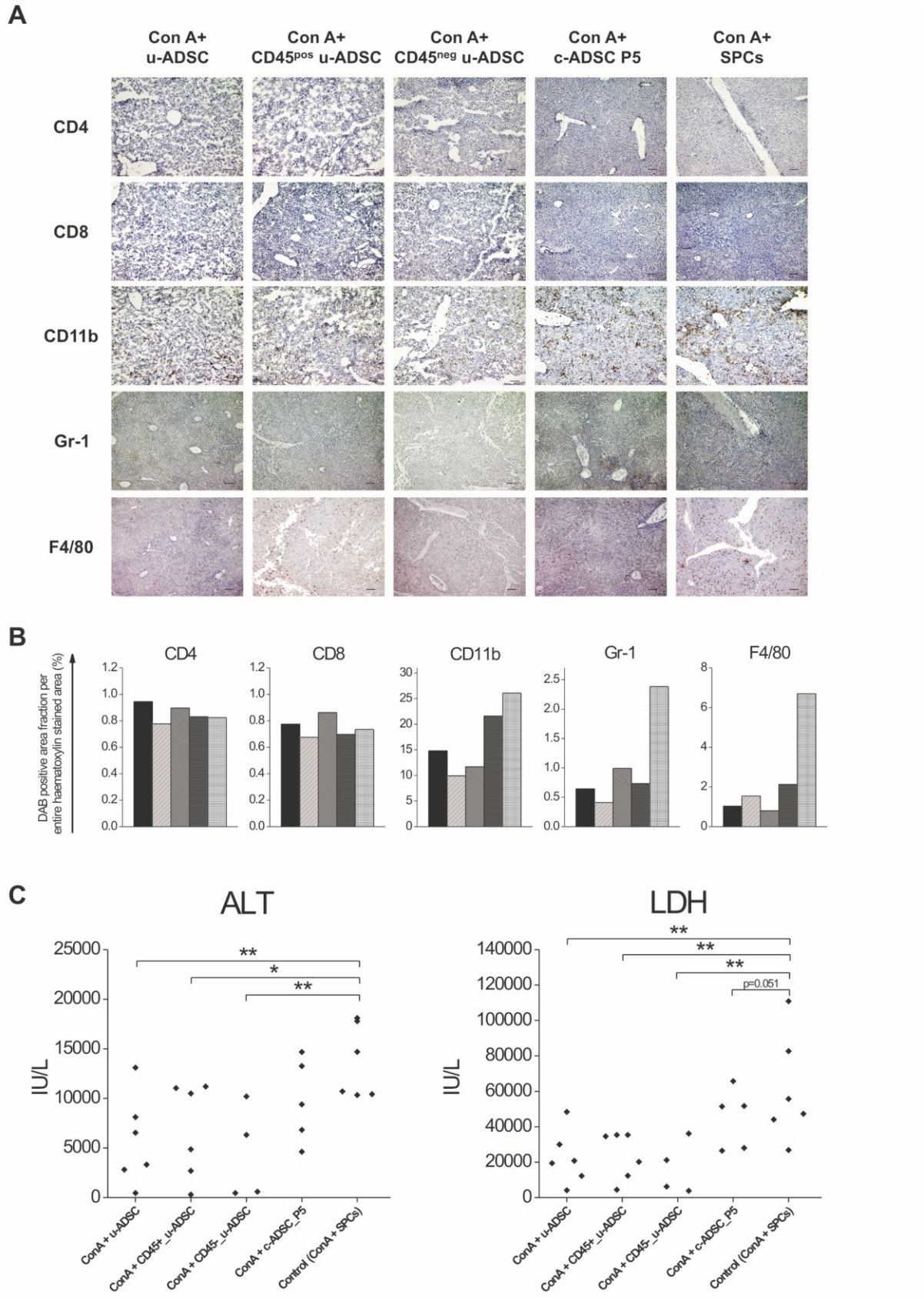
A
Con A+ u-ADSC
Con A+ CD45pos u-ADSC
Con A+ CD45neg u-ADSC
Con A+ c-ADSC P5
Con A+ SPCs
CD4
CD8
CD11b
Gr-1
F4/80
B
DAB positive area fraction per entire haematoxylin stained area (%)
CD4
CD8
CD11b
Gr-1
F4/80
C
ALT
LDH
IU/L
p=0.051
ConA + u-ADSC
ConA + CD45+ u-ADSC
ConA + CD45- u-ADSC
ConA + c-ADSC_P5
Control (ConA + SPCs)

FIGURE 3.

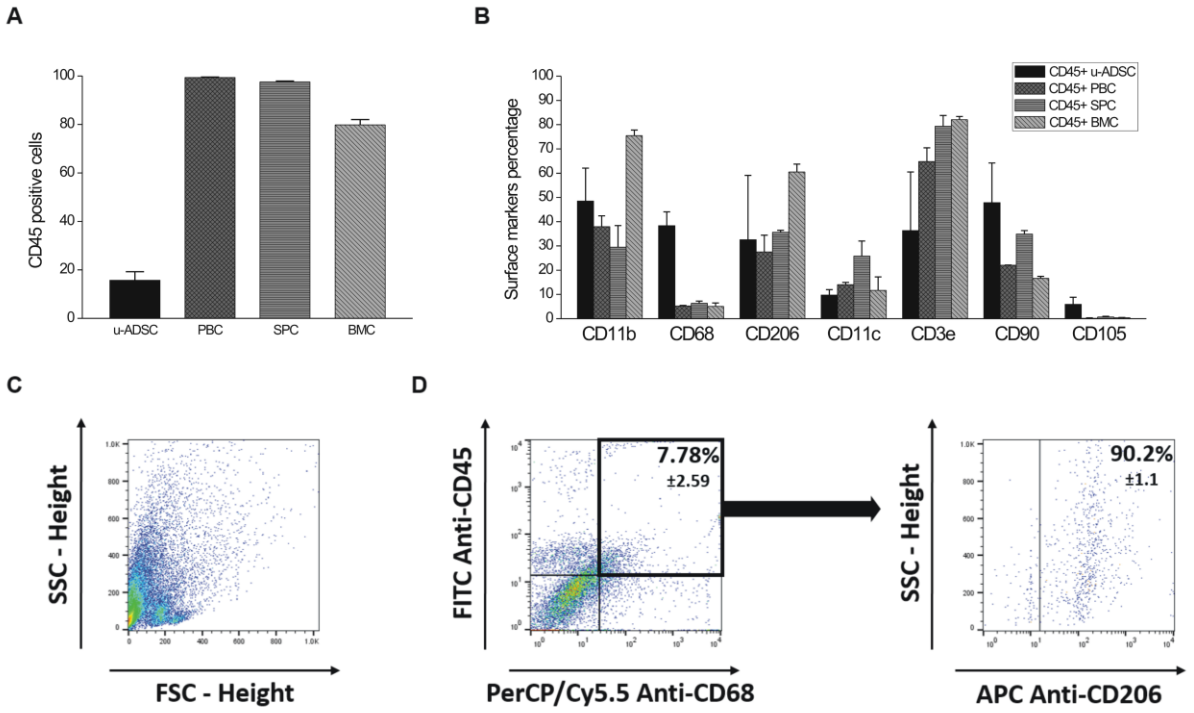

FIGURE 4.

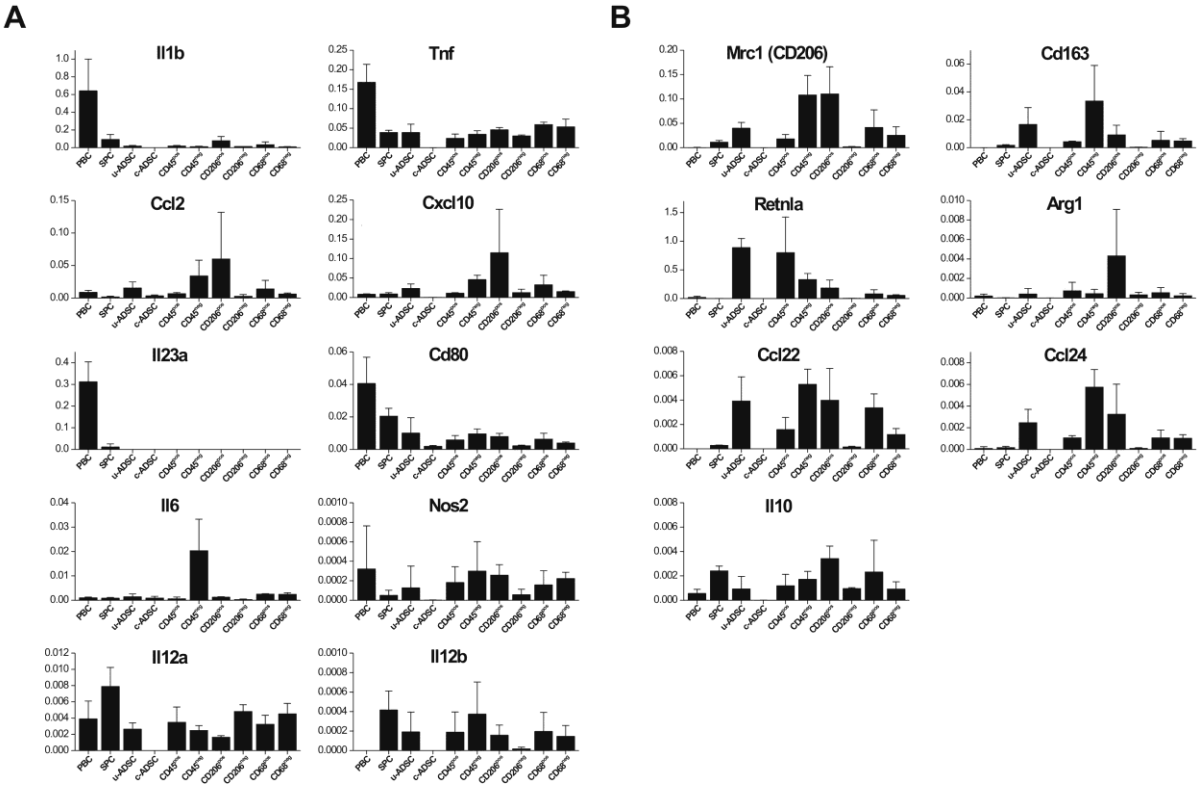

FIGURE 5.

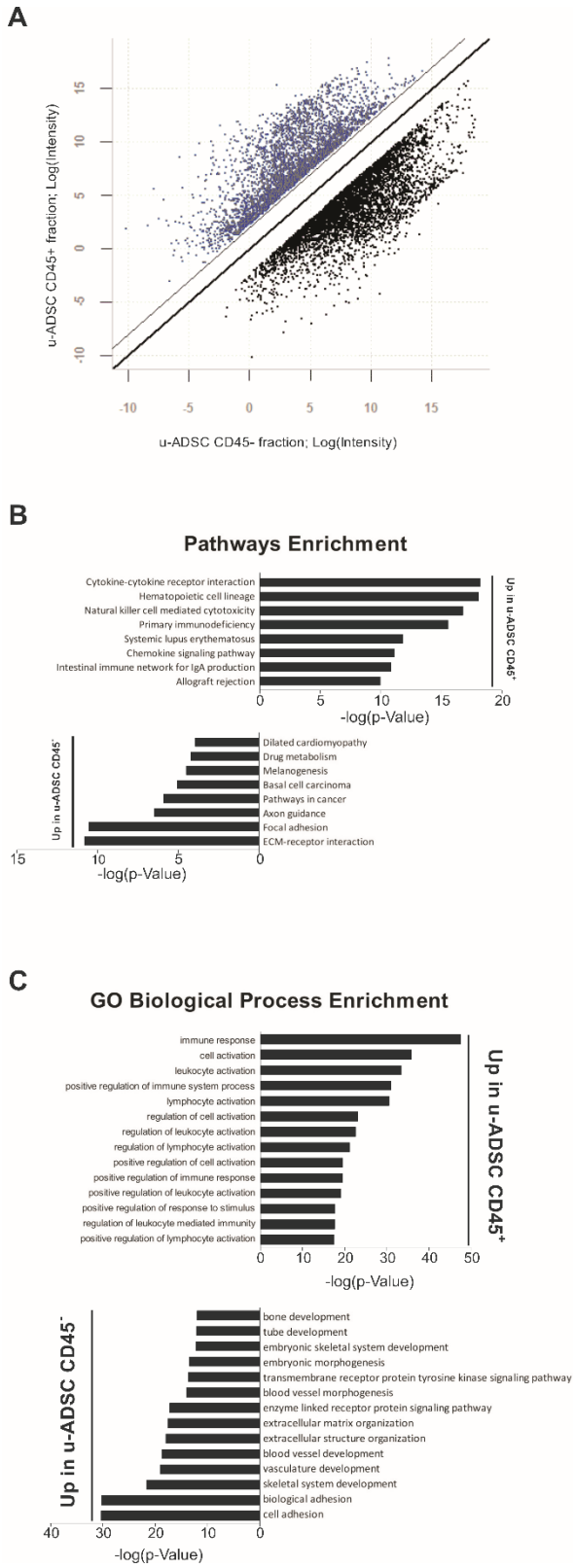
A
u-ADSC CD45+ fraction; Log(Intensity)
u-ADSC CD45- fraction; Log(Intensity)
B
Pathways Enrichment
Cytokine-cytokine receptor interaction
Hematopoietic cell lineage
Natural killer cell mediated cytotoxicity
Primary immunodeficiency
Systemic lupus erythematosus
Chemokine signaling pathway
Intestinal immune network for IgA production
Allograft rejection
Up in u-ADSC CD45+
-log(p-Value)
Dilated cardiomyopathy
Drug metabolism
Melanogenesis
Basal cell carcinoma
Pathways in cancer
Axon guidance
Focal adhesion
ECM-receptor interaction
Up in u-ADSC CD45-
-log(p-Value)
C
GO Biological Process Enrichment
immune response
cell activation
leukocyte activation
positive regulation of immune system process
lymphocyte activation
regulation of cell activation
regulation of leukocyte activation
regulation of lymphocyte activation
positive regulation of cell activation
positive regulation of immune response
positive regulation of leukocyte activation
positive regulation of response to stimulus
regulation of leukocyte mediated immunity
positive regulation of lymphocyte activation
Up in u-ADSC CD45+
-log(p-Value)
bone development
tube development
embryonic skeletal system development
embryonic morphogenesis
transmembrane receptor protein tyrosine kinase signaling pathway
blood vessel morphogenesis
enzyme linked receptor protein signaling pathway
extracellular matrix organization
extracellular structure organization
blood vessel development
vasculature development
skeletal system development
biological adhesion
cell adhesion
Up in u-ADSC CD45-
-log(p-Value)

FIGURE 6.

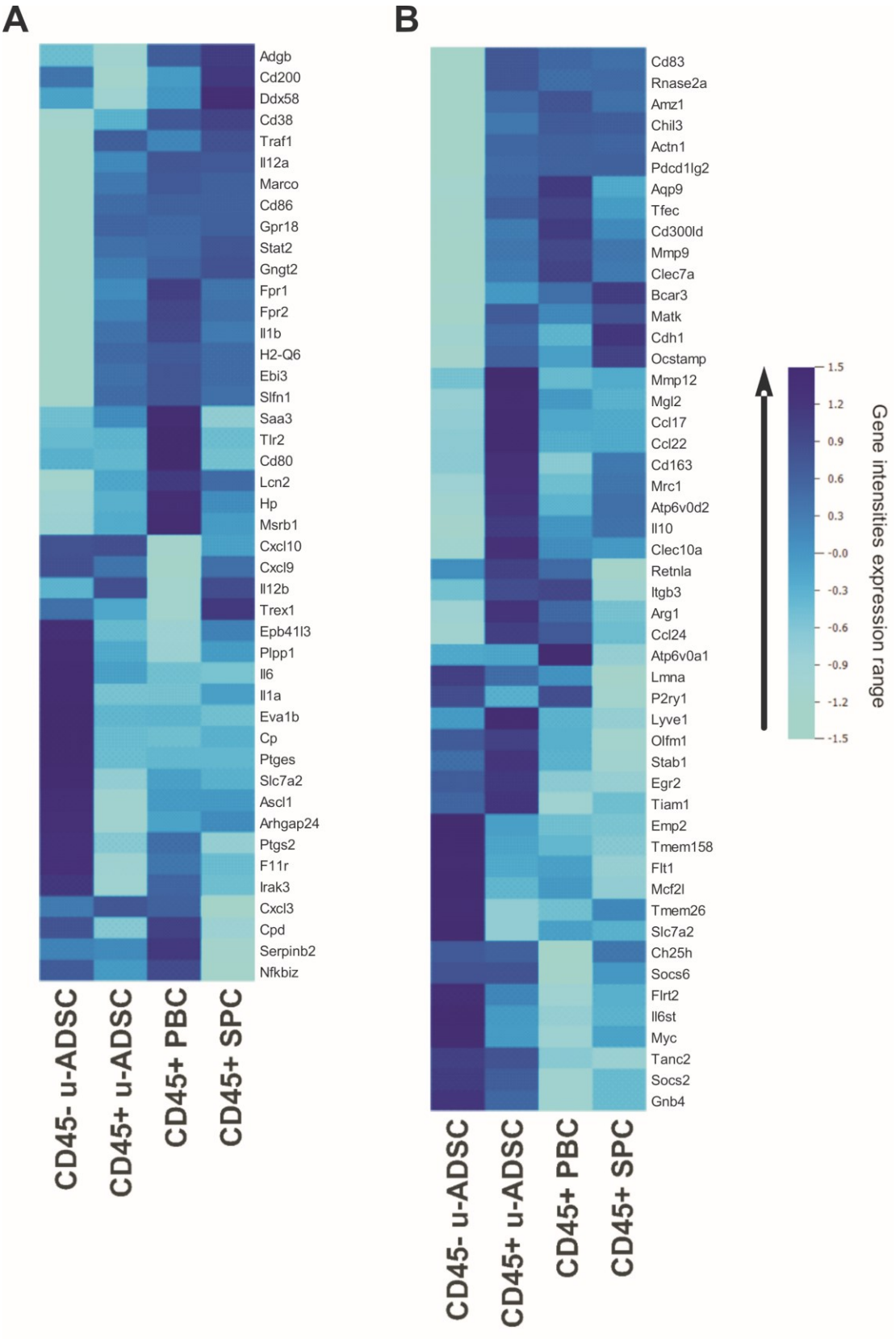
A
Adgb
Cd200
Ddx58
Cd38
Traf1
Il12a
Marco
Cd86
Gpr18
Stat2
Gngt2
Fpr1
Fpr2
Il1b
H2-Q6
Ebi3
Slfn1
Saa3
Tlr2
Cd80
Lcn2
Hp
Msrb1
Cxcl10
Cxcl9
Il12b
Trex1
Epb41l3
Plpp1
Il6
Il1a
Eva1b
Cp
Ptges
Slc7a2
Ascl1
Arhgap24
Ptgs2
F11r
Irak3
Cxcl3
Cpd
Serpinb2
Nfkbiz
CD45- u-ADSC
CD45+ u-ADSC
CD45+ PBC
CD45+ SPC
B
Cd83
Rnase2a
Amz1
Chil3
Actn1
Pdcd1lg2
Aqp9
Tfec
Cd300ld
Mmp9
Clec7a
Bcar3
Matk
Cdh1
Ocstamp
Mmp12
Mgl2
Ccl17
Ccl22
Cd163
Mrc1
Atp6v0d2
Il10
Clec10a
Retnla
Itgb3
Arg1
Ccl24
Atp6v0a1
Lmna
P2ry1
Lyve1
Olfm1
Stab1
Egr2
Tiam1
Emp2
Tmem158
Flt1
Mcf2l
Tmem26
Slc7a2
Ch25h
Socs6
Flrt2
Il6st
Myc
Tanc2
Socs2
Gnb4
CD45- u-ADSC
CD45+ u-ADSC
CD45+ PBC
CD45+ SPC
1.5
1.2
0.9
0.6
0.3
-0.0
-0.3
-0.6
-0.9
-1.2
-1.5
Gene intensities expression range

FIGURE 7.

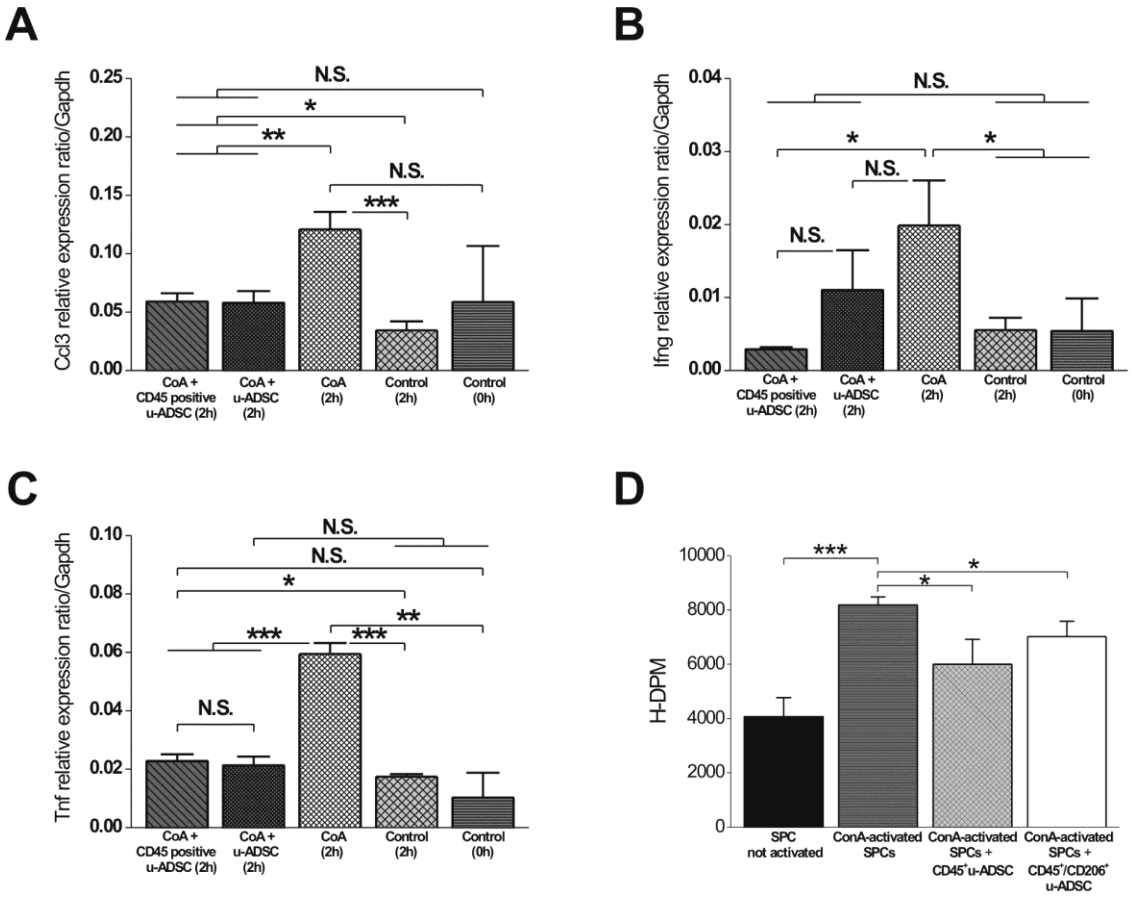
A
Ccl3 relative expression ratio/Gapdh
0.25
0.20
0.15
0.10
0.05
0.00
N.S.
*
**
N.S.
***
CoA + CD45 positive u-ADSC (2h)
CoA + u-ADSC (2h)
CoA (2h)
Control (2h)
Control (0h)
B
Ifng relative expression ratio/Gapdh
0.04
0.03
0.02
0.01
0.00
N.S.
*
*
N.S.
N.S.
CoA + CD45 positive u-ADSC (2h)
CoA + u-ADSC (2h)
CoA (2h)
Control (2h)
Control (0h)
C
Tnf relative expression ratio/Gapdh
0.10
0.08
0.06
0.04
0.02
0.00
N.S.
N.S.
*
**
***
***
N.S.
CoA + CD45 positive u-ADSC (2h)
CoA + u-ADSC (2h)
CoA (2h)
Control (2h)
Control (0h)
D
H-DPM
10000
8000
6000
4000
2000
0
***
*
*
SPC not activated
ConA-activated SPCs
ConA-activated SPCs + CD45+u-ADSC
ConA-activated SPCs + CD45+/CD206+ u-ADSC